Chapter 4
Fluorescence Detection System

Tao G. Nelson, Glen D. Ramsay, and Matthew A. Perugini

Abstract One of the most exciting advances in contemporary analytical ultracentrifugation has been the development of the analytical ultracentrifuge equipped with a fluorescence detection system (AU-FDS). The AU-FDS provides both selectivity and sensitivity thereby enabling the measurement of specific fluorescently labeled macromolecules in complex solutions and/or the detection of dilute samples at low (sub-nanomolar) concentrations. This has had tremendous impact to the study of low-abundance proteins, the quantification of high-affinity interactions ($K_D < nM$), and the characterization of biomolecules in crowded biological backgrounds. This chapter will describe the (i) development, (ii) optical setup, (iii) advantages and disadvantages, (iv) pre-experimental requirements, (v) experimental operation procedures, and (vi) contemporary applications of the AU-FDS focused on enzyme self-association, antibody-antigen interactions, amyloid protein aggregation, and the composition of enzyme complexes.

Keywords Analytical ultracentrifugation • Analytical ultracentrifuge • Fluorescence detection system • Fluorescence optics • Green fluorescent protein • High affinity • Interaction • Sedimentation • Sensitive • Selective

4.1 Development of the Fluorescence Detection System

The basic principle of analytical ultracentrifugation (AUC) requires the detection of a sample or analyte as a function of radial position and time in a gravitational field established by the force of centrifugation (Cole et al. 2008; Howlett et al. 2006; Kroe and Laue 2009). Historically, this was first achieved by Svedberg in the 1920s using colloidal particles and proteins measured by schlieren optics (Svedberg and Pedersen 1940), which earned him the 1926 Nobel Prize in Chemistry. Rayleigh

T.G. Nelson • M.A. Perugini (✉)
Department of Biochemistry and Genetics, La Trobe Institute for Molecular Science, La Trobe University, Melbourne, VIC 3086, Australia
e-mail: M.Perugini@latrobe.edu.au

G.D. Ramsay
Aviv Biomedical, Inc, Lakewood, NJ 08701, USA

S. Uchiyama et al. (eds.), *Analytical Ultracentrifugation*,
DOI 10.1007/978-4-431-55985-6_4

interference optics were then developed by Schachman and colleagues in the 1950s for the Spinco Model E instrument (Schachman 1959; van Holde and Hansen 1998) and later advanced to the contemporary interference optical system of the Beckman XL-I instrument through the developmental work of Yphantis, Laue, and colleagues (Yphantis et al. 1994). Toward the end of the twentieth century, an absorbance detector was developed for the Beckman XL-A instrument (Giebeler 1992; Laue 1996), which enabled the analysis of nucleic acids, proteins, and biomolecular complexes through the detection of native chromophores. At the beginning of the twenty-first century, it was also Laue and his colleagues at the University of New Hampshire that developed the fluorescence detection system (FDS) for the Beckman XL-A/XL-I instruments (Laue et al. 1997; Laue and Stafford 1999; Laue 2004; MacGregor et al. 2004), although a fluorescence detector for the Model E was earlier described by Riesner and co-workers (Schmidt et al. 1990). The development of the FDS provided several technical challenges, including the engineering of complex electronics, optics, temperature stabilization, and a high-flux laser source. However, Laue and colleagues were able to resolve these issues through precision engineering and the utilization of a solid-state laser and black body radiation (Laue 2004; MacGregor et al. 2004). The FDS is now commercially available from Aviv Biomedical, who provide the hardware, Advanced Operating System (AOS) data acquisition software, and technical assistance.

4.2 FDS Optical Setup

The Aviv Biomedical FDS is purchased separately and fitted into the vacuum chamber of the Beckman XL-A/XL-I (Fig. 4.1a), where it is positioned above the rotor mounted with sample cell(s) (Fig. 4.1b). The basic assembly of the fluorescence optics is configured similar to that of a confocal microscope with coaxial excitation and emission (Fig. 4.1c). Light is emitted from a laser (originally a solid-state laser, now a diode laser) tuned to 488 nm, which is reflected at right angles by a mirror and expanded into a cone to a collimating lens (Fig. 4.1c). The collimated light is then directed by a dichroic mirror to the sample cell where the excitation beam is focused by a condensing lens that also functions as the objective lens for the emission beam (Fig. 4.1c). The excited fluorescently labeled sample will then emit light at longer wavelengths (>488 nm), which passes through the dichroic mirror to a cutoff filter that restricts transmission to wavelengths between 505 and 565 nm. Finally, the filtered emission beam is refocused by a lens through a 50 μm pin hole and then to the photomultiplier tube (PMT) (Fig. 4.1c). The resulting emission signal is measured as a function of radial position across the sample cell using a stepper motor capable of progressing in 20 μm steps (Cole et al. 2008; MacGregor et al. 2004). Similar to interference and absorbance measurements, the signal (in this case fluorescence intensity) versus radial position is then measured at different time points enabling the monitoring and subsequent analysis of the sedimenting (or floating) fluorescently labeled analyte.

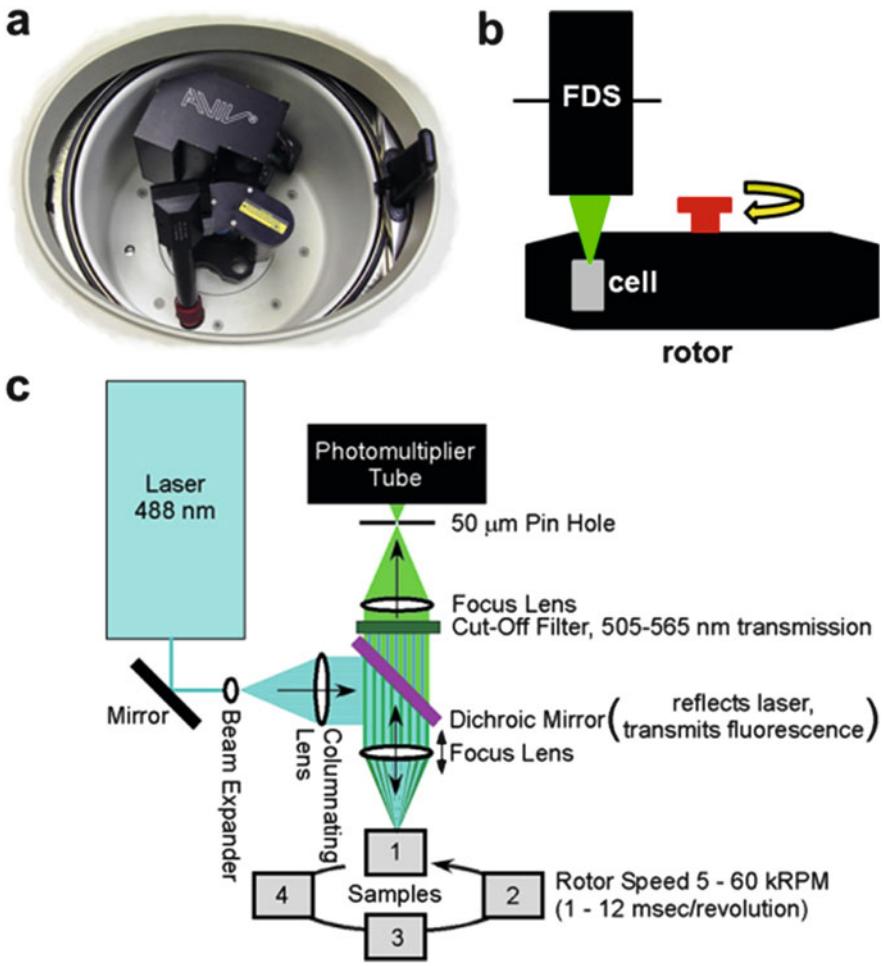

Fig. 4.1 The AU-FDS hardware. (**a**) The inside of a Beckman XL-I analytical ultracentrifuge fitted with the FDS optics box and Beckman Coulter absorbance – interference detector. (**b**) Diagrammatical representation showing the side view of the FDS optics positioned above the rotor and sample cell. (**c**) The optical path of the FDS from laser to photomultiplier tube (PMT)

4.3 Advantages and Limitations

The FDS provides significant advantages over the more conventional interference and absorbance optics. Firstly, the fluorescence detector offers 2–3 orders of magnitude higher sensitivity, which equates to the detection of picomolar concentrations of fluorescently labeled sample (Table 4.1). This capability is referred to as *normal use tracer sedimentation* (NUTS) (Kroe and Laue 2009). By contrast, absorbance or interference optics can only detect, at best, low nanomolar sample concentrations

Table 4.1 Comparison of absorbance, interference, and fluorescence optics for the analytical ultracentrifuge

Detector	Absorbance	Interference	Fluorescence
Sensitivity[a]	0.1 OD	0.1 mg/ml	100 pM
Dynamic range[b]	2–3 logs	3–4 logs	6–8 logs
K_D lower limit[c]	nM	nM	pM
Selectivity[d]	No	No	Yes
Sample throughput[e]	1–7	1–7	1–14
Perturbation of analyte required for detection	No	No	Yes[f]

[a]Minimum amount of sample required to obtain a good signal
[b]Concentration range of analyte
[c]Lowest magnitude for accurate measurement of binding affinity
[d]Specific detection of an analyte in complex or crowded solutions
[e]Number of samples per experiment (upper range using an eight-hole An-50Ti rotor)
[f]Requires labeling of analyte with a suitable fluorophore (e.g., Alexa Fluor 488 or green fluorescent protein)

(Table 4.1). Practically, the increased sensitivity of the AU-FDS affords the quantification of tight biomolecular interactions with sub-nanomolar dissociation constants (K_D) (Table 4.1) (Burgess et al. 2008; Kroe and Laue 2009; Zhao et al. 2013, 2014b). Another advantage of the FDS is the selective detection of trace amounts of analyte in complex or crowded biological solutions, such as plasma, urine, cerebrospinal fluid, or cell lysates (Table 4.1). This capability has been coined *biological online tracer sedimentation* (BOLTS) (Kroe and Laue 2009). However, the AU-FDS requires conjugation of a fluorophore in order to afford sample detection. This represents a potential limitation, since the attachment of a fluorescent partner can perturb the native properties of the analyte of interest (Romanini and Cornish 2012) (Table 4.1). By comparison, absorbance and interference optics enable the measurement of native, non-modified biomolecules (Table 4.1). Nevertheless, the AU-FDS offers greater sample throughput given that no reference solution is required (Kroe and Laue 2009). This means that both compartments of a standard double-sector cell can be occupied by sample. Accordingly, a maximum of 6 samples (when using a four-hole rotor) and 14 samples (when using an eight-hole rotor) can be accommodated in the AU-FDS per experiment, compared to only 3 and 7 samples, respectively, when using absorbance or interference optics (Table 4.1).

4.4 Pre-experimental Requirements

4.4.1 Sample Labeling

As discussed in Sect. 4.3, one of the inherent requirements of the AU-FDS is the attachment of an appropriate fluorescent probe to the sample of interest. Given that the laser is tuned to 488 nm, the selection of a fluorescent partner is limited

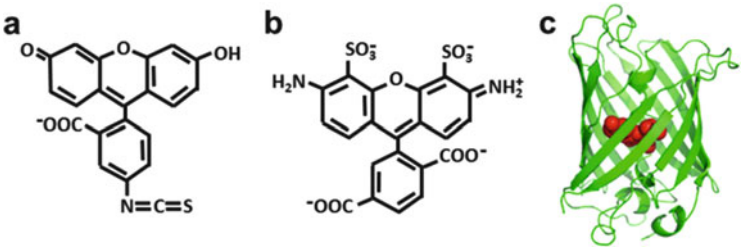

Fig. 4.2 Structures of common fluorophores used in the AU-FDS. (**a**) Fluorescein isothiocyanate (FITC), (**b**) Alexa Fluor 488, and (**c**) *green* fluorescent protein (GFP) (PDB ID: 1EMA)

to fluorophores with an excitation spectrum encompassing this wavelength. It is therefore common to use fluorescein derivatives, such as fluorescein isothiocyanate (Fig. 4.2a) and Alexa Fluor 488 (Fig. 4.2b). Alexa Fluor 488 is an excellent choice due to its high quantum yield, resistance to photobleaching, and stability over a broad pH range (Cole et al. 2008). Furthermore, Alexa Fluor 488 is commercially available in succinimidyl ester or maleimide coupling chemistries to afford efficient conjugation to native amine or thiol groups of biomolecules, respectively (Bailey et al. 2009; Burgess et al. 2008). As an example, a three-step protocol for producing 1:1 labeled protein for the AU-FDS has been developed by Bailey and colleagues (Bailey et al. 2009). Firstly, the protein is incubated with amine-reactive Alexa Fluor 488 succinimidyl ester. Free dye is then removed using a desalting column, which also buffer exchanges, and finally, a hydrophobic column is employed to separate the labeled and unlabeled biomolecules. This method can easily be adapted to label cysteine (i.e., thiol)-containing proteins using the Alexa Fluor 488 maleimide preparation.

Sample labeling can also be achieved via attachment of CyX dyes to hexa-histidine (His) tags of recombinantly expressed proteins (Hellman et al. 2011; Zhao et al. 2010). This offers another advantage of the hexa-histidine tag in addition to its traditional use in protein purification using immobilized metal-affinity chromatography (Hochuli et al. 1988; Zhao et al. 2010). Alternatively, labeling can be achieved via coupling of the sample to green fluorescent protein (GFP) (Fig. 4.2c) (Kroe and Laue 2009), which is a native fluorescent gene product originally isolated from the jellyfish *Aequorea victoria* (Tsien 1998). Commercial vectors producing GFP fusion proteins are now widely available for all types of expression systems enabling AU-FDS users to prepare recombinant proteins as GFP fusion constructs (Polling et al. 2013). However, native GFPs possess the propensity to dimerize in solution (Campbell et al. 2002), which can bias studies aimed at characterizing the quaternary structure of GFP-tagged constructs. To circumvent this, several monomeric analogs of GFP have recently been engineered, including red and blue fluorescent varieties (Campbell et al. 2002; Pettikiriarachchi et al. 2012; Wilmann et al. 2005). The use of photoswitchable versions of GFP commonly employed in super-resolution microscopy is also feasible in the AU-FDS (Zhao et al. 2014a)

4.4.2 Meniscus Detection

In order to calculate accurate sedimentation coefficients in the analytical ultracentrifuge, one needs to know the radial position of the meniscus (i.e., the air/water interface) in the sample sector (Bailey et al. 2009; Zhao et al. 2014b). This represents the origin of sedimentation. With absorbance or interference optics, the meniscus can easily be determined since an obvious spike in the signal is observed at the air/water interface. However, given that the AU-FDS measures fluorescence just below the surface of the sample, there is no opportunity for light to scatter. Accordingly, the position of the sample meniscus is not easily recognizable in radial scans generated in the AU-FDS. One solution developed by Bailey and co-workers is to overlay the sample with light mineral oil containing an uncharged fluorescent dye such as BODIPY 493/503 (Bailey et al. 2009). This produces a clear signal at the oil/water interface that correlates to the origin of sedimentation. More recently, Schuck and colleagues describe an alternative method for determining the meniscus position in the AU-FDS using the Raman scattering profile of water (Zhao et al. 2014b). This method works well at high PMT voltages, since Raman scattering of water results in a baseline signal shift at the radius corresponding to the air/water interface (Zhao et al. 2014b).

4.4.3 Sample Loading

As for absorbance- or interference-detected measurements, samples to be analyzed in the AU-FDS are loaded into double-sector cells fitted with either quartz or sapphire windows pre-torqued to 120 psi. As documented in Sect. 4.3, a reference solution is not required, which enables the user to load sample into both compartments when using conventional double-sector cells. The cells are sealed from the external environment using Teflon plugs and brass screws in the same manner employed for absorbance or interference measurements. Each cell is then loaded into either a Beckman An-60 Ti four-hole rotor or Beckman An-50 Ti eight-hole rotor. However, instead of using a counterbalance as employed for absorbance or interference measurements, a special purpose-built calibration centerpiece is required. This centerpiece has the same weight as a two-channel epon or charcoal centerpiece but contains a fluorescent strip with known dimensions. Given that it has the same weight as a two-channel centerpiece, no counterweight is required. The rotor containing sample cells and calibration centerpiece is then mounted in the AU-FDS ready for experiment initiation.

4.5 Experimental Operation Procedures

The following subsections will present a basic overview of experimental operation of the AU-FDS. It is not the intention here to describe a complete standard operation procedure for the instrument, since this is provided by Aviv Biomedical upon purchase of the FDS optics unit and AOS software. Instead, the proceeding subsections will focus on some of the unique operational features, common problems, and strategies the user can adopt to manage or circumvent these problems.

4.5.1 Experiment Initiation

Both the FDS detector and XL-A/XL-I centrifuge are controlled by the AOS software. When the software is initiated, the *rotor setup* panel appears (Fig. 4.3). Additional panels are available to configure the experiment and select cells for data collection. The AU-FDS enjoys a large dynamic range of up to five magnitudes in fluorescence intensity. This is made possible given the powerful laser source, high-sensitivity detector, high-voltage PMT, and the addition of an adjustable amplifier (Fig. 4.1c). Both the PMT voltage and the amplifier's gain can be adjusted to levels that are optimal for each sample. When samples have more than a magnitude

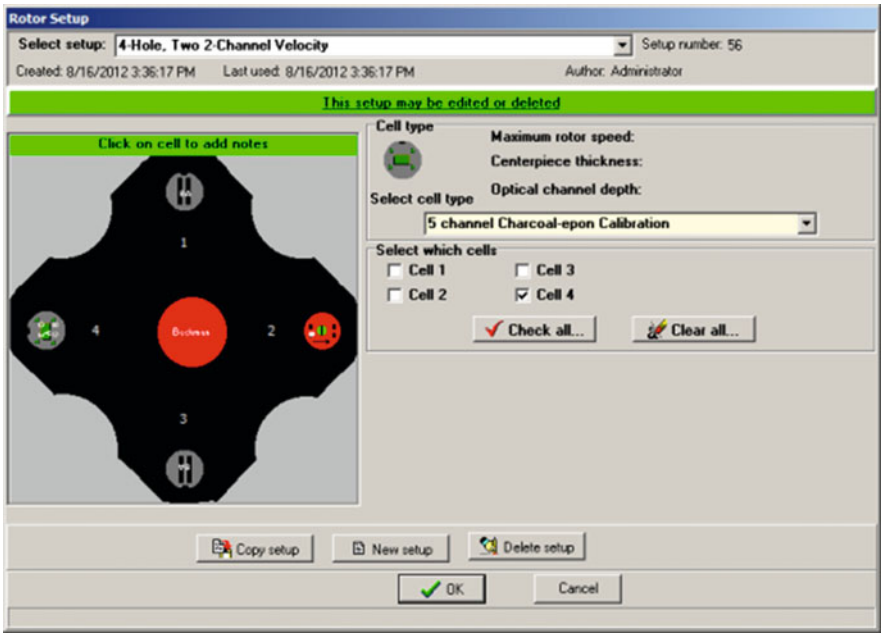

Fig. 4.3 Rotor setup screen of the AOS software

difference in fluorescent intensity, experiments can be performed with more than one set of sensitivities. However, each gain setting requires additional radial scans, which attenuates the rate of data collection. Accordingly, most experiments in the AU-FDS, particularly sedimentation velocity studies, are conducted with a single gain setting to afford maximum scan rates of ∼90 s per sample.

4.5.2 Position Calibration

To measure concentration gradients in the analytical ultracentrifuge, the optical system must be able to accurately determine the position of the signal. This is achieved in the AU-FDS using a cylindrical coordinate system described by an "angle," "radius," and "height."

The "angle" is dependent on the rotor velocity and is adjusted automatically by AOS. When the rotor speed changes, AOS applies an algorithm that searches for the fluorescent strip in the calibration centerpiece. The AOS software then applies an angle offset so that the center of the strip falls in the expected angular range. This process is referred to as "locking the magnet angle."

The "radius" can be adjusted automatically or manually. This is achieved by performing a radial calibration via the *fluorescence focusing and calibration tool* panel of AOS (Fig. 4.4). The high-radius edge of the fluorescent strip serves as the reference point. A radial calibration should be performed at least monthly, when the rotor is changed or when maintenance is performed.

The "height" refers to the position of the focal point of the excitation beam, which is adjusted by moving the vertical position of the focus lens located above the sample cell (Fig. 4.1c). This is also adjusted in the *fluorescence focusing and calibration tool* panel of AOS (Fig. 4.4). The "focus height" is critical in the AU-FDS given the conical shape of the beam (Fig. 4.1c). The adjustment range is broad, since the focus point of the beam can be positioned from just above the sample solution to well below the surface, therefore encompassing the 12 mm path length of a standard double-sector centerpiece. For dilute samples (less than 0.1 optical density/cm), the focal point profile is sigmoidal (Fig. 4.5, 13 pM IgG). Moreover, little fluorescence is observed when the focus point is located above the sample; but as this is shifted deeper into the sample, a transition region is observed followed then by a signal plateau (Fig. 4.5, 13 pM IgG). To achieve maximum signal and stability, the focus point should be set to the starting portion of the plateau. It should be noted that the 4 mm height sample cells are too short for the focal point to be fully encompassed, since it begins to leave the bottom of the sample before it has fully entered the top. As a result, focus scans of these cells produce only a peak, never a plateau; therefore 4 mm cells do not provide the full sensitivity of 12 mm cells. Furthermore, Beckman Coulter 4 mm cells have a top surface below the height of the 12 mm cells, resulting in increased clipping at the high-radius edge (see Sect. 4.5.3.2 for clipping details).

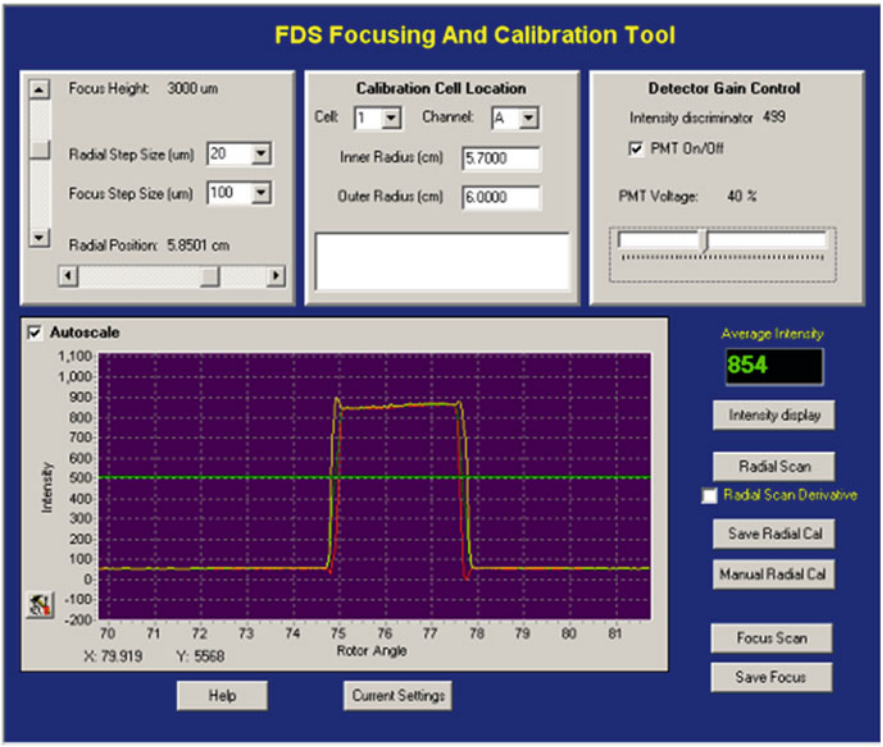

Fig. 4.4 FDS focusing and calibration tool screen of AOS

4.5.3 Common Signal Attenuation Issues

The optical nature of the FDS can give rise to common phenomena that result in attenuation of the signal, namely, (i) the "inner filter effect," (ii) "light beam clipping," and (iii) "focal height drift." The strategies employed to circumvent these potential problems will be discussed below.

4.5.3.1 Inner Filter Effect

At high concentrations of fluorescently labeled sample (>0.1 optical density/cm), significant absorption of incident and emitted light results. This is known as the "inner filter effect" (Lyons et al. 2013). A practical rule of thumb is that if the sample has a color seen by the eye, then it is at risk of having an inner filter effect. In the AU-FDS, inner filtering occurs when the focal depth is moved deeper into a sample solution that absorbs, whether it be due to the fluorophore, sample, or other buffer components. What results is a characteristic sigmoidal profile followed then by an

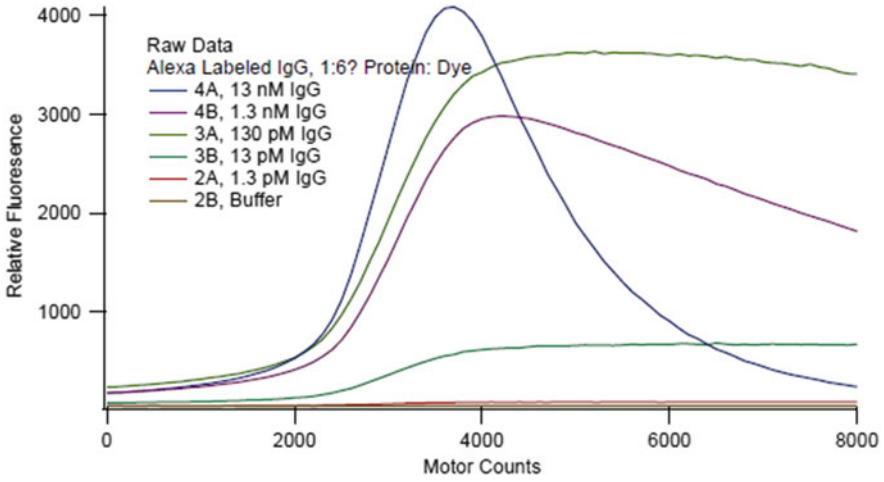

Fig. 4.5 Focus scans of Alexa Fluor 488-labeled IgG at different loading concentrations. The PMT high voltages were adjusted to keep the signal strengths in range of the electronics. As a result, the signal amplitude is not necessarily proportionate to the concentration between samples

exponential decrease in light intensity as the focus height is moved deeper into the sample (Fig. 4.5, 13 nM IgG). Intuitively, one would predict that inner filtering could be prevented in the AU-FDS by raising the focal height of the beam closer to the sample surface. However, this is avoided in practice, since the change in sample concentration during sedimentation (or flotation) results in deeper penetration of the laser light causing a change in the focus profile. This introduces nonlinearity of the signal as a function of sample concentration. Accordingly, the best method to avoid inner filtering in the AU-FDS is to reduce the label concentration of the fluorescent sample at higher sample concentrations. Moreover, concentration-dependence studies should simply employ a fixed concentration of labeled sample but an increase in the proportion of unlabeled sample (Wowor et al. 2011). As such, all samples in the concentration series will have similar fluorescence levels. Importantly, this approach will also afford the use of a single gain setting thus maximizing the rate of data collection (Sect. 4.5.1). In summary, the best way to manage the inner filter effect in the AU-FDS is to prevent it from occurring.

4.5.3.2 Light Beam Clipping

Given that the excitation beam in the AU-FDS is conical in shape, light emerging from the first focus lens to the top of the sample can be "clipped" by the edge of the cell (Fig. 4.1c). This results in attenuation of the fluorescence signal. By comparison, the light beam emerging from the absorbance and interference systems is columnar in shape and therefore is unaffected by movements in the light beam. Clipping can occur in two physical locations. First, the edges of the sample channels

can clip the light if the focus is set too deep in the sample. This situation reduces the period of time the sample is clearly viewed during a rotation. To circumvent this problem, the focal point of the beam is positioned at the beginning of the focus scan plateau (Fig. 4.5). This also prevents focal height drift (Sect. 4.5.3.3). The second source of clipping is even more prominent at the high-radius (i.e., wider) end of the sample sector, due to the cell's retaining ring. However, this clipping can be mitigated by using a dense oil (such as FC-43) to raise the sample off the bottom of the cell (Bailey et al. 2009). Alternatively, a special FDS two-channel velocity cell with a slightly shorter column height is available to purchase from Spin Analytical (www.spinanalytical.com).

4.5.3.3 Focal Height Drift

Since the optical path in the FDS is not perfectly parallel to the sample surface, a slight drift of the focus height occurs during radial scans. Hence, if the focus height is placed on a sloping portion of the focus scan (Fig. 4.5), the slight vertical drift of the optics results in a signal change. Nevertheless, setting the focal point to the plateau region of the focus scan prevents this drift from occurring.

4.5.4 Data Acquisition and Analyses

Once the user has optimized the fluorescence signal for each sample and programmed the experiment method to be followed, the experiment is commenced by hitting START in the AOS main experiment window (Fig. 4.6). Temperature equilibration can be handled manually or can be included as part of the experiment method. The rotor will then accelerate until the input speed is attained at which point data collection will commence. Each scan is then measured as a function of time and plotted by the AOS software to allow the user to view all time points (Fig. 4.6). The experiment is then stopped after a predetermined time/number of scans or manually by the user when all samples have sedimented to the bottom (or floated to the top) of the cell. The AOS software packages the data in time-stamped files that are available for analysis using contemporary software suites, such as SEDANAL (Stafford and Sherwood 2004), SEDFIT (Schuck 2000; Schuck et al. 2002), SEDPHAT (Vistica et al. 2004), and ULTRASCAN (Demeler 2005). Both sedimentation velocity and equilibrium types of experiments are possible.

4.5.5 Post-experimental Considerations

The post-experiment procedures of the AU-FDS do not differ substantially from those employing absorbance or interference optics. However, the detergent used for

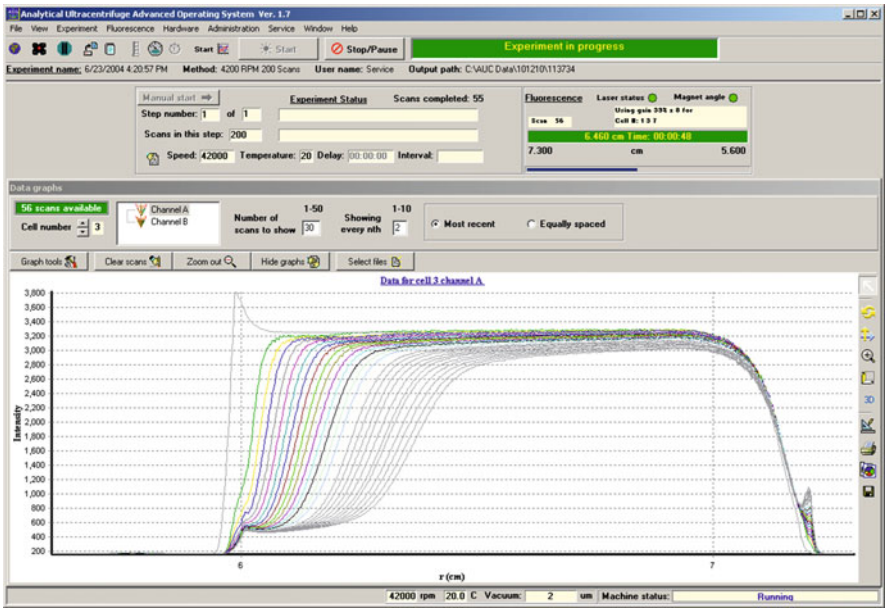

Fig. 4.6 AOS main experiment screen showing fluorescence intensity versus radial position profile of a sample at different time points

cleaning cells is critical, since many household detergents contain high amounts of fluorescein. As a consequence, we have found that trace amounts of these detergents remaining in cleaned cells can give rise to a non-sedimenting baseline in the AU-FDS. However, this problem can be avoided by using a natural detergent, which is colorless or pale yellow in appearance, compared to fluorescein-containing products that have a bright fluorescent green color.

4.6 Applications of AU-FDS

4.6.1 High-Affinity Interactions

As documented in Sect. 4.3, one of the major advantages of the AU-FDS platform is the ability to quantify high-affinity or tight interactions (Table 4.1). To illustrate this in the context of protein self-association, Burgess and colleagues employed the AU-FDS to study and quantify the self-association of a tight dimeric enzyme from the gram-positive pathogen *Staphylococcus aureus* (also refer to Chap. 16). The enzyme, dihydrodipicolinate synthase (DHDPS) (Fig. 4.7a), is of significant interest to biomedicine given that it is the product of an essential bacterial gene that is absent in humans (Dogovski et al. 2013; Kobayashi et al. 2003). Accordingly,

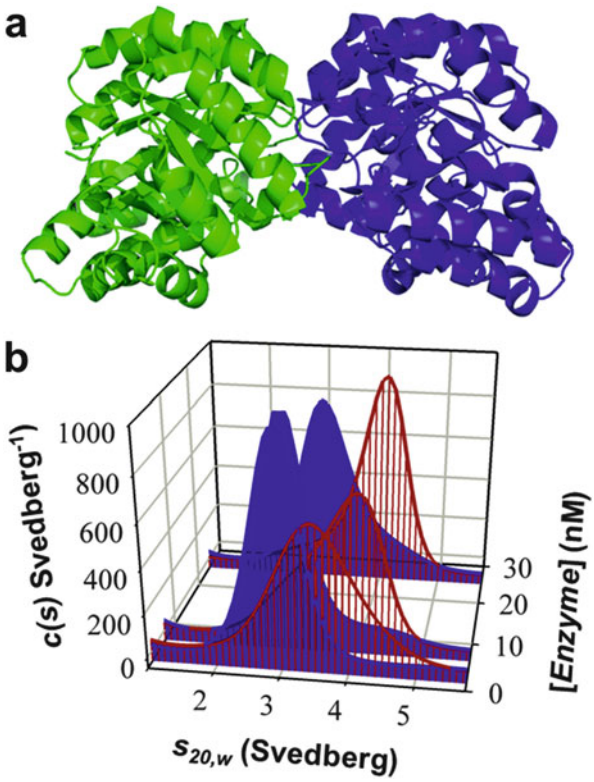

Fig. 4.7 AU-FDS studies of a high-affinity dimeric enzyme. (**a**) Structure of *S. aureus* DHDPS dimer (PDB ID: 3DAQ). (**b**) Continuous size-distribution [*c(s)*] analyses of *S. aureus* DHDPS plotted as a function of standardized sedimentation coefficient and enzyme concentration. The distributions for the apoenzyme are shown in *blue*, whereas the profiles in the presence of pyruvate are displayed in *red*

DHDPS represents a valid but as yet unexploited antibiotic target (Dogovski et al. 2009, 2012; Gerrard et al. 2007; Hutton et al. 2007). The study by Burgess et al. (2008) commenced with absorbance-detected AUC measurements at low micromolar enzyme concentrations. The resulting sedimentation velocity data, which was analyzed using enhanced van Holde-Weischet (Demeler and van Holde 2004) and continuous size-distribution (Schuck 2000; Schuck et al. 2002) algorithms, demonstrated that *S. aureus* DHDPS exists as a 4.2 S dimeric species. The dimer was shown to be highly stable at enzyme concentrations ranging from mid- to low micromolar in either the apo (i.e., unliganded) or substrate-bound forms. However, sedimentation velocity experiments conducted in the AU-FDS using Alexa Fluor 488-labeled enzyme at high picomolar to low nanomolar concentrations showed that *S. aureus* DHDPS actually exists in a monomer-dimer equilibrium (Fig. 4.7b). Interestingly, the addition of the substrate, pyruvate, shifted the equilibrium in favor of the dimer (Fig. 4.7b). Although pyruvate absorbs strongly in the ultraviolet region, which limits its use in absorbance-detected AUC experiments, saturating (i.e., mM) concentrations of pyruvate were able to be employed in this study, since the substrate is nonfluorescent and thus did not contribute to the signal derived from the Alexa Fluor 488-labeled enzyme. Subsequent sedimentation equilibrium studies

were then conducted at high picomolar to low nanomolar enzyme concentrations in the absence and presence of pyruvate to show that the dimer-monomer dissociation constant ($K_D^{2\rightarrow1}$) was 33 nM for the apoenzyme but 20-fold tighter in the presence of pyruvate (i.e., $K_D^{2\rightarrow1} = 1.6$ nM). The dimerization affinity determined by AU-FDS was subsequently validated using enzyme kinetics assays that determined the concentration dependence on the specific activity of *S. aureus* DHDPS (Burgess et al. 2008). This was made possible since the *S. aureus* DHDPS monomer is significantly less active than the dimer (Burgess et al. 2008). The Burgess et al. (2008) study was one of the first to employ AU-FDS to quantify a high-affinity interacting system and provide an example of both NUTS and BOLTS applications of the technique (Sect. 4.3). Subsequent studies have also employed the platform to quantify high-affinity interactions, including self-associating proteins (Wowor et al. 2011; Zhao et al. 2012), antibody-antigen interactions (Kroe and Laue 2009; Zhao et al. 2014b), and protein-RNA interactions (Husain et al. 2012).

4.6.2 Studies in Complex Backgrounds

The use of absorbance-detected AUC provides a convenient method for measuring sedimentation. While this is a powerful technique for purified samples, the nonspecific nature of protein absorption makes absorbance-detected AUC inappropriate in complex or heterogeneous sample backgrounds. As discussed in Sect. 4.3, the BOLTS application of AU-FDS makes it possible to characterize the hydrodynamic properties of a fluorescently labeled macromolecule in biological fluids, such as blood serum and cell lysates (Table 4.1). As will be seen below, these more complex solutions can change the behavior of the macromolecule of interest, and so observations made using simpler buffers may not predict the true behavior of biomolecules in vivo. However, when assessing the behavior of protein drugs (such as monoclonal antibodies) or studying protein aggregation linked to common age-related diseases (such as systemic amyloidosis), it is critical to understand how proteins behave in biological fluids.

4.6.2.1 Behavior of Protein Therapeutics in Blood Serum

The importance of studying biomolecules in biological fluids was highlighted by Demeule et al. (2009) who showed that proteins can form different quaternary structures in plasma than they do in phosphate-buffered saline (PBS). Demeule et al. (2009) reasoned that while much in vitro work is conducted to assess the properties of protein drugs, little is known of their properties in the bloodstream, due in part to the expense and difficulty of conducting animal and clinical studies. One such drug is omalizumab, an anti-IgE monoclonal antibody used in the treatment of asthma (Liu et al. 1995). Earlier work had shown that omalizumab formed different complexes with IgE when the omalizumab/IgE molar ratio was varied

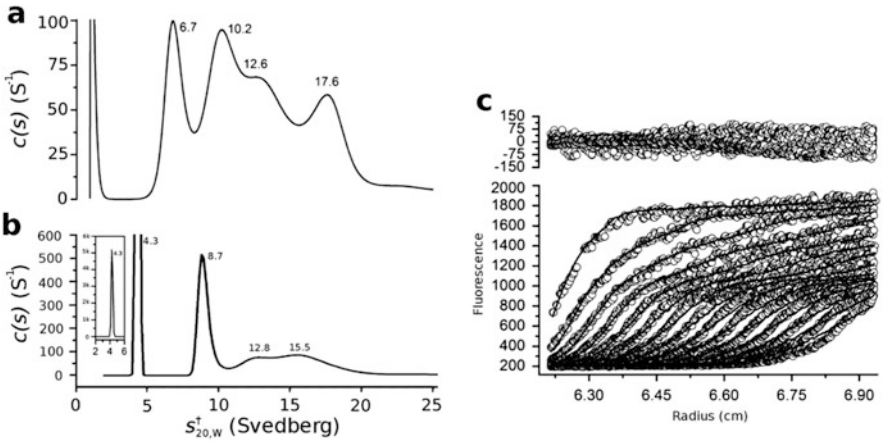

Fig. 4.8 AU-FDS analysis of antibody complexes in serum. *c(s)* distributions for omalizumab-IgE complexes in (**a**) PBS and (**b**) serum where $s^{\dagger}_{20,w}$ is the apparent corrected sedimentation coefficient. The distribution in serum shows substantially more monomers (8.7 S) than oligomers, compared to the distribution in PBS. The 4.3 S species (panel (**b**) inset) is attributed to albumin. (**c**) Data (*symbols*) and fits (*lines*) for the *c(s)* distribution best fit in serum (refer to panel (**b**)). Residuals are shown above plotted as a function of radial position (Figure adapted from Demeule et al. (2009))

(Liu et al. 1995). Demeule and colleagues therefore set out to employ AU-FDS to further explore these antibody-antigen interactions. Omalizumab was labeled with Alexa Fluor 488, mixed in PBS buffer with IgE in equimolar concentrations, and then added to human serum. The hydrodynamic properties of the mixture in serum (Fig. 4.8b) compared to the PBS control (Fig. 4.8a) were determined by sedimentation velocity studies. The *c(s)* distribution analyses showed that substantial differences exist between the omalizumab-IgE complexes in buffer and serum, with higher levels of monomer (8.7 S species) observed in the more complex background of serum. The 4.3 S species (Fig. 4.8b) is attributed to albumin, which has been shown to bind endogenous fluorescent molecules, highlighting that AU-FDS data generated in serum must be carefully interpreted. The nonlinear regression least squares output for the *c(s)* distribution in serum showed that the residuals are systematic and larger than the random noise (Fig. 4.8c), indicating that the *c(s)* distribution model does not perfectly model the data. The bulk density and viscosity of serum were employed in these analyses to determine the apparent corrected sedimentation coefficient ($s^{\dagger}_{20,w}$) of the various species. Although the authors acknowledge that this may produce inaccuracies, the resulting $s^{\dagger}_{20,w}$ values actually matched those determined in PBS. This study was one of the first to provide proof of concept that the hydrodynamic properties of fluorescently labeled macromolecules can be determined in complex biological backgrounds using the AU-FDS.

4.6.2.2 Aggregation of Serum Proteins Linked to Systemic Amyloidosis

The nature of complex formation in biological fluids is of particular interest in the study of amyloid diseases, such as Alzheimer's disease, Parkinson's disease, Huntington's disease, and systemic amyloidosis, since it is yet to be established whether protein aggregates observed in these diseases are pathogenic or merely symptomatic (Swart et al. 2014). In the case of senile systemic amyloidosis (SSA), the primary cause of death for 70 % of supercentenarians (Coles and Young 2012), the disease is manifested by the aggregation of transthyretin (TTR), which normally functions as a tetramer to transport thyroid hormone in the bloodstream. It is unknown how TTR transitions between a physiologically active soluble tetramer to a disease-associated amyloid-like aggregate, but it is generally assumed that the first step involves dissociation of the tetramer (Coles and Young 2012). To examine the aggregation of TTR, Kingsbury et al. (2008) conducted sedimentation velocity experiments in the AU-FDS using recombinant TTR labeled with fluorescein that was subsequently added to human serum. Similar to the aforementioned studies of omalizumab (Sect. 4.6.2.1), the *c(s)* distribution best fit of TTR in serum resulted in large systematic residuals (Fig. 4.9a). This once again indicates that the *c(s)* distribution model (Schuck 2000; Schuck et al. 2002) does not appropriately account for the nonideality in the complex background of serum. Nevertheless, the resulting *c(s)* distribution (at a confidence interval of 68 %) yielded a single peak with a sedimentation coefficient of 2.41 S, which is consistent with the size found by boundary midpoint analysis (2.45 S) (Fig. 4.9b). Kingsbury et al. (2008) therefore argue that although investigating protein aggregation in complex solutions is somewhat confounded by current analysis approaches, AU-FDS is a valuable platform to study protein aggregation ex vivo. However, the outputs using current

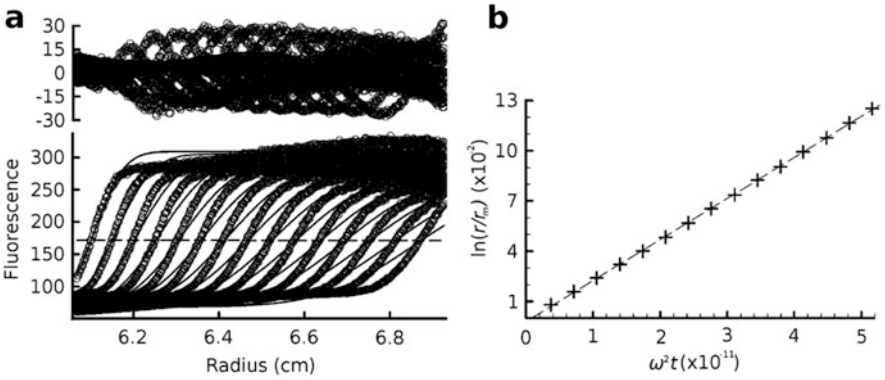

Fig. 4.9 AU-FDS studies of transthyretin aggregation in serum. (**a**) Data (*symbols*) and fits (*lines*) resulting from the *c(s)* distribution best fit of TTR in serum resulting in a single peak with sedimentation coefficient of 2.41 S (distribution not shown). Residuals are plotted above as a function of radial position. (**b**) Boundary midpoint analysis for the data shown in panel (a) yields a single species of 2.45 S (Figure adapted from Kingsbury et al. (2008))

data analysis methods, such as *c(s)* distribution analysis, should be observed in a more qualitative rather than quantitative manner.

Kingsbury et al. (2012) subsequently set out to explore a second aggregating system, namely, immunoglobulin light chain, which is associated with another form of systemic amyloidosis known as light chain amyloidosis (AL). AL is the most common form of systemic amyloidosis and the most life threatening, particularly when cardiomyopathy presents (Sanchorawala 2006). It is caused by unregulated light chain production by plasma cells and, if left untreated, can induce pathogenic changes in many systems including the hepatic, digestive, peripheral nervous, and cardiovascular system (Sanchorawala 2006). In the study by Kingsbury et al. (2012), serum was collected from patients suffering from systemic amyloidosis and classed into one of four clinical groups, namely, (i) no amyloidosis, (ii) SSA, (iii) AL without cardiomyopathy (AL), and (iv) AL with cardiomyopathy (AL-CMP). A high concentration of albumin was used as a negative control. As adopted in the TTR study described earlier (Kingsbury et al. 2008), fluorescein was used as the tracer for BOLTS experiments in the AU-FDS. The fluorophore was simply added to the serum samples collected from individual patients. The resulting sedimentation profiles of the four groups showed that the samples could be clearly differentiated into two types, designated type 1 or type 2. Type 1 samples displayed only one boundary with a sedimentation coefficient of 2.1–3.3 S, comparable to the fluorescein-bound albumin control (2.3 S) (Fig. 4.10a, c). However, type 2 samples were heterogeneous with two major high-molecular-weight complexes (HMWCs) with sedimentation coefficients of 5.8 S and 10.8 S (Fig. 4.10b, d). The additional inverted slow-moving boundary observed in the type 2 sample (Fig. 4.10b) is consistent with the Johnston-Ogston effect, which is a sedimentation artifact arising from nonideal boundaries (Johnston and Ogston 1946). All four clinical groups displayed the type 1 profile, but type 2 patterns were only observed in samples displaying amyloidosis, suggesting that HMWCs are a hallmark of disease. Furthermore, HMWCs were detected in over half of the AL-CMP samples and less often in AL and SSA, correlating with AL-CMP being the most life-threatening form. This supports the notion that HMWCs may play a role in pathogenesis. Interestingly, the addition of recombinant TTR to SSA patient serum increased the levels of HMWCs, suggesting that the HMWCs observed in systemic amyloidosis are associated with TTR. As with the study by Kingsbury et al. (2008) reported earlier, the *c(s)* distribution model provides a poor description of the data. This is likely to be due to time-dependent spreading of the boundary resulting from the high-density gradient presenting in the centrifuge due to the complex nature of serum. Although this prevented the determination of accurate molecular weights for the HMWCs, the sedimentation coefficients derived via Lamm equation modeling approximated to that determined by boundary midpoint migration. Despite these limitations, AU-FDS has allowed the first observations of high-molecular-weight complexes in the serum of patients suffering systemic amyloidosis.

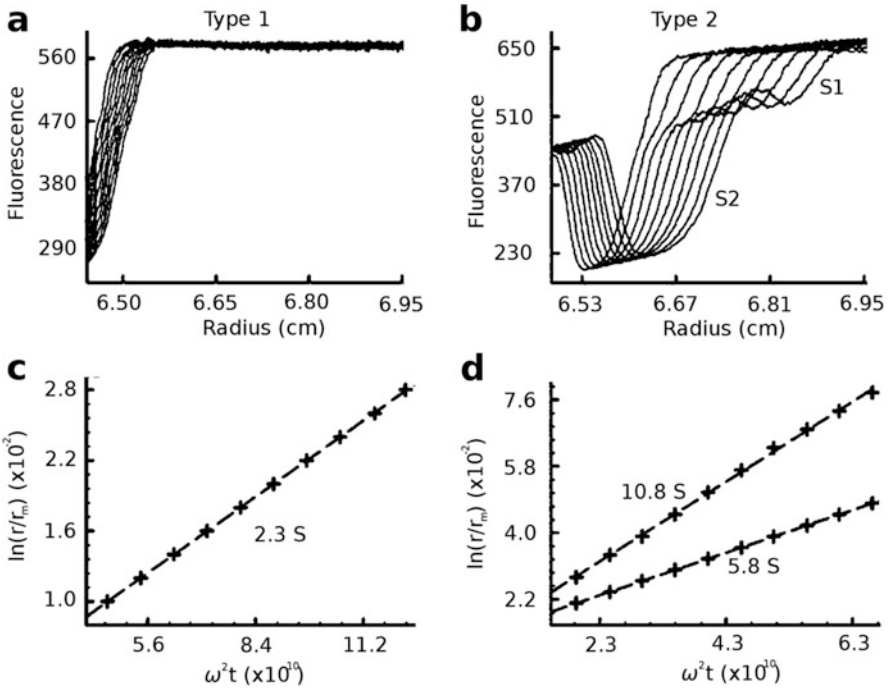

Fig. 4.10 AU-FDS analysis of high-molecular-weight complexes in serum from patients with systemic amyloidosis. Fluorescence intensity is plotted as a function of radial position for (**a**) type 1 and (**b**) type 2 samples, with the resulting midpoint boundary analyses shown in panels (**c**) and (**d**), respectively. Based on the sedimenting boundaries shown, patient samples can be grouped into type 1 or type 2 (Figure adapted from Kingsbury et al. (2012))

4.6.2.3 Aggregation of Huntingtin in Cell Lysates

AU-FDS has also been employed to study protein aggregation of huntingtin (Htt) protein associated with Huntington's disease (Olshina et al. 2010). This is an autosomal dominant condition caused by the addition of repeated CAG codons in exon 1 of the huntingtin gene, which results in poly-glutamine (poly-Q)-rich mutant huntingtin proteins (Landles and Bates 2004). Olshina et al. (2010) investigated Htt aggregation in the AU-FDS by studying Htt containing 46 glutamine repeats (Htt46Q) as a GFP fusion protein in aqueous buffer and also in mouse neuroblastoma (Neuro2a) cell lysates. In buffer, the recombinant Htt46Q-GFP construct was shown to exist as a 2.4 S monomer that aggregated over time to form 100 to 6000 S complexes. By contrast, AU-FDS studies of Htt46Q-GFP in Neuro2a cell lysates harvested at different transfection time points showed that three distinct species are present, namely, 2.3 S monomer, 140 S soluble oligomer, and 320,000 S inclusion bodies (Fig. 4.11). Interestingly, the relative amount of 2.3 S monomer decreases over time, while the proportion of 320,000 S inclusion bodies increase

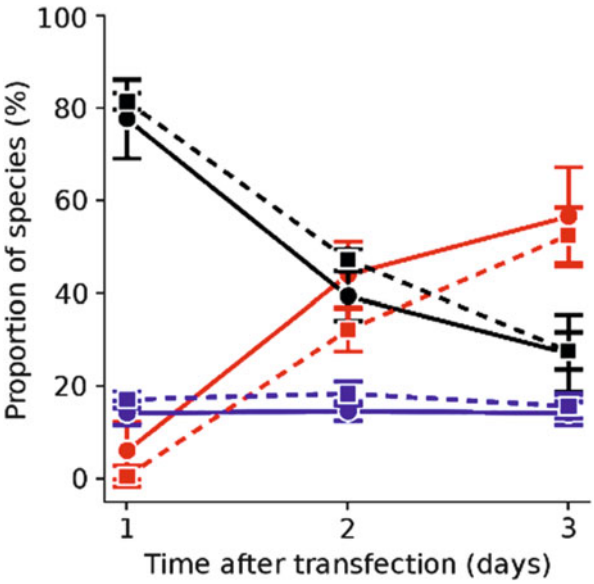

Fig. 4.11 AU-FDS experiments of huntingtin aggregates in cell lysates. Proportions of different species of Htt46Q-GFP in Neuro2a cell lysates are plotted as a function of transfection time. *Black*, monomer (2.3 S); *blue*, oligomer (140 S); and *red*, inclusion bodies (320,000 S). *Dotted* and *solid lines* indicate the absence and presence, respectively, of Hsc70 (Figure adapted from Olshina et al. (2010))

and the amount of 140 S oligomer remains constant (Fig. 4.11). This suggests that the 140 S species represents a rate-limiting factor in aggregation. Studies were also conducted in the presence of Hsc70, which is a member of the heat shock protein 70 (Hsp70) chaperone family that is known to co-localize with inclusion bodies and lower Htt toxicity (Warrick et al. 1999). AU-FDS experiments conducted in Neuro2a cell lysates containing overexpressed Hsc70 show that the relative proportion of soluble oligomers decrease while the proportion of inclusion bodies increase (Fig. 4.11, solid lines). This suggests that Hsp70 reduces Htt toxicity by facilitating the conversion of soluble oligomers into inclusion bodies. Accordingly, this study yielded critical insights into the molecular mechanisms underpinning pathogenesis in Huntington's disease.

4.6.3 Identifying Enzyme Complexes

In addition to the aforementioned NUTS and BOLTS applications of AU-FDS, Wang et al. (2012) have recently employed the technology to explore the size and composition of enzyme complexes functioning in translation from the model organism, *Saccharomyces cerevisiae*. By tagging specific proteins or RNA with GFP and performing a pulldown with FLAG-labeled large ribosomal subunit protein RPL25A or poly(A)-binding protein PAB1, Wang et al. were able to identify a new 77 S monosomal translation complex. Akin to Western blotting, this AU-FDS application showed that the complex is comprised of the 80S ribosome, mRNA, PAB1, and eukaryotic initiation factors, eIF4E and eIF4G (Wang et al.

2012). Additional experiments conducted in a separate study demonstrate that the complex also contains eRF1, SLF1, SSD1, PUB1, and SBP1 (Zhang et al. 2014). Further, Wang et al. (2012) probed the mechanisms by which environmental stress inhibits translation. This study showed that glucose starvation leads to a substantial reduction of 77 S complex abundance, an effect that is partially rescued by mutations in eIF4E and eIF3b or by deletion of PAT1 but not by mutations in PAB1. This suggests that glucose starvation acts through eIF4E. By contrast, amino acid deprivation, osmotic stress, and heat shock are not rescued, suggesting they do not act primarily through this complex (Wang et al. 2012).

4.7 Conclusions

The recent development of the fluorescence detection system for the analytical ultracentrifuge (AU-FDS) has provided significant advances to the hydrodynamic and thermodynamic analyses of macromolecular systems. This platform technology provides *sensitivity* for the measurement of low-abundance proteins and the quantitation of tight biomolecular interactions (NUTS applications), as well as *selectivity* for the specific detection of a biomolecule of choice in complex biological backgrounds (BOLTS applications). In this chapter, we have described studies of tight self-associating enzymes (DHDPS), protein therapeutics (omalizumab), and amyloid-like aggregating proteins (TTR, immunoglobulin light chain, and huntingtin) to demonstrate NUTS and BOLTS applications of the AU-FDS. We also describe the use of the technology for proteomic investigations, such as defining the composition of the 77 S monosomal translation complex. This highlights the great diversity of the platform in this, the post-genome era, where the emphasis has switched from the delineation of genome structure and the characterization of isolated gene products to the qualitative and quantitative measurement of gene product interaction networks in complex in vivo-like backgrounds. However, several challenges remain for the advancement of the AU-FDS, including the development of multiwavelength excitation laser sources to permit the use of a broader range of fluorescent probes and advancement of analytical tools to circumvent nonideality observed in complex biological fluids. Nevertheless, the AU-FDS provides researchers with a cutting edge tool for contemporary applications of macromolecular characterization in solution.

References

Bailey MF, Angley LM, Perugini MA (2009) Methods for sample labeling and meniscus determination in the fluorescence-detected analytical ultracentrifuge. Anal Biochem 390(2):218–220

Burgess BR, Dobson RCJ, Bailey MF, Atkinson SC, Griffin MDW, Jameson GB, Parker MW, Gerrard JA, Perugini MA (2008) Structure and evolution of a novel dimeric enzyme from a clinically-important bacterial pathogen. J Biol Chem 283(41):27598–27603

Campbell RE, Tour O, Palmer AE, Steinbach PA, Baird GS, Zacharias DA, Tsien RY (2002) A monomeric red fluorescent protein. Proc Natl Acad Sci U S A 99(12):7877–7882

Cole JW, Lary JW, Moody TP, Laue TM (2008) Analytical ultracentrifugation: sedimentation velocity and sedimentation equilibrium. In: Correia JJ, Detrich H (eds) Methods in cell biology, vol 84. Elsevier, San Diego, pp 143–179

Coles LS, Young RD (2012) Supercentenarians and transthyretin amyloidosis: the next frontier of human life extension. Prev Med 54:S9–S11

Demeler B (2005) UltraScan a comprehensive data analysis software package for analytical ultracentrifugation experiments. In: Scott DJ, Harding SE, Rowe AJ (eds) Modern analytical ultracentrifugation: techniques and methods. Royal Society of Chemistry, Cambridge, pp 210–229

Demeler B, van Holde KE (2004) Sedimentation velocity analysis of highly heterogeneous systems. Anal Biochem 335(2):279–288

Demeule B, Shire SJ, Liu J (2009) A therapeutic antibody and its antigen form different complexes in serum than in phosphate-buffered saline: a study by analytical ultracentrifugation. Anal Biochem 388(2):279–287

Dogovski C, Atkinson S, Dommaraju S, Dobson RCJ, Hor L, Hutton CA, Gerrard JA, Perugini MA (2009) Lysine biosynthesis in bacteria: an unchartered pathway for novel antibiotic design. In: Doelle HW, Rokem S (eds) Encyclopedia of life support systems, vol 11. Encyclopedia of Life Support Systems (EOLSS). Developed under the Auspices of the UNESCO, EOLSS Publishers, Paris, pp 116–136

Dogovski C, Atkinson SC, Dommaraju SR, Downton M, Hor L, Moore S, Paxman JJ, Peverelli MG, Qiu TW, Reumann M, Siddiqui T, Taylor NL, Wagner J, Wubben JM, Perugini MA (2012) Enzymology of bacterial lysine biosynthesis. In: Ekinci D (ed) Biochemistry. InTech Open Access Publisher, Rijeka, pp 225–262

Dogovski C, Gorman MA, Ketaren NE, Praszkier J, Zammit LM, Mertens HD, Bryant G, Yang J, Griffin MD, Pearce FG, Gerrard JA, Jameson GB, Parker MW, Robins-Browne RM, Perugini MA (2013) From knock-out phenotype to three-dimensional structure of a promising antibiotic target from *Streptococcus pneumoniae*. PLoS ONE 8(12):e83419

Gerrard JA, Hutton CA, Perugini MA (2007) Inhibiting protein-protein interactions as an emerging paradigm for drug discovery. Mini Rev Med Chem 7(2):151–157

Giebeler R (1992) The optima XL-A: a new analytical ultracentrifuge with a novel precision absorption optical system. In: Harding SE, Rowe AJ, Horton JC (eds) Analytical ultracentrifugation biochemistry and polymer science. Royal Society of Chemistry, Cambridge, pp 16–25

Hellman LM, Zhao C, Melikishvili M, Tao X, Hopper JE, Whiteheart SW, Fried MG (2011) Histidine-tag-directed chromophores for tracer analyses in the analytical ultracentrifuge. Methods 54(1):31–38

Hochuli E, Bannwarth W, Döbeli D, Gentz R, Stüber D (1988) Genetic approach to facilitate purification of recombinant proteins with a novel metal chelate adsorbent. Nat Biotech 6(11):1321–1325

Howlett GJ, Minton AP, Rivas G (2006) Analytical ultracentrifugation for the study of protein association and assembly. Curr Opin Chem Biol 10(5):430–436

Husain B, Mukerji I, Cole JL (2012) Analysis of high-affinity binding of protein kinase R to double-stranded RNA. Biochemistry 51(44):8764–8770

Hutton CA, Perugini MA, Gerrard JA (2007) Inhibition of lysine biosynthesis: an evolving antibiotic strategy. Mol Biosyst 3(7):458–465

Johnston JP, Ogston AG (1946) A boundary anomaly found in the ultracentrifugal sedimentation of mixtures. Trans Faraday Soc 42:789–799

Kingsbury JS, Laue TM, Klimtchuk ES, Theberge R, Costello CE, Connors LH (2008) The modulation of transthyretin tetramer stability by cysteine 10 adducts and the drug diflunisal: direct analysis by fluorescence-detected analytical ultracentrifugation. J Biol Chem 283(18):11887–11896

Kingsbury JS, Laue TM, Chase SF, Connors LH (2012) Detection of high-molecular-weight amyloid serum protein complexes using biological on-line tracer sedimentation. Anal Biochem 425(2):151–156

Kobayashi K, Ehrlich SD, Albertini A, Amati G, Andersen KK, Arnaud M, Asai K, Ashikaga S, Aymerich S, Bessieres P, Boland F, Brignell SC, Bron S, Bunai K, Chapuis J, Christiansen LC, Danchin A, Debarbouille M, Dervyn E, Deuerling E, Devine K, Devine SK, Dreesen O, Errington J, Fillinger S, Foster SJ, Fujita Y, Galizzi A, Gardan R, Eschevins C, Fukushima T, Haga K, Harwood CR, Hecker M, Hosoya D, Hullo MF, Kakeshita H, Karamata D, Kasahara Y, Kawamura F, Koga K, Koski P, Kuwana R, Imamura D, Ishimaru M, Ishikawa S, Ishio I, Le Coq D, Masson A, Mauel C, Meima R, Mellado RP, Moir A, Moriya S, Nagakawa E, Nanamiya H, Nakai S, Nygaard P, Ogura M, Ohanan T, O'Reilly M, O'Rourke M, Pragai Z, Pooley HM, Rapoport G, Rawlins JP, Rivas LA, Rivolta C, Sadaie A, Sadaie Y, Sarvas M, Sato T, Saxild HH, Scanlan E, Schumann W, Seegers JF, Sekiguchi J, Sekowska A, Seror SJ, Simon M, Stragier P, Studer R, Takamatsu H, Tanaka T, Takeuchi M, Thomaides HB, Vagner V, van Dijl JM, Watabe K, Wipat A, Yamamoto H, Yamamoto M, Yamamoto Y, Yamane K, Yata K, Yoshida K, Yoshikawa H, Zuber U, Ogasawara N (2003) Essential *Bacillus subtilis* genes. Proc Natl Acad Sci U S A 100(8):4678–4683

Kroe RR, Laue TM (2009) NUTS and BOLTS: applications of fluorescence-detected sedimentation. Anal Biochem 390(1):1–13

Landles C, Bates GP (2004) Huntingtin and the molecular pathogenesis of Huntington's disease. EMBO Rep 5(10):958–963

Laue TM (1996) Optical systems of the XLA ultracentrifuge. Applications data note for Spinco division of Beckman Instruments. Beckman Instruments Inc, Palo Alto

Laue TM (2004) Analytical ultracentrifugation: a powerful 'new' technology in drug discovery. Drug Discov Today Technol 1(3):309–315

Laue TM, Stafford WF (1999) Modern applications of analytical ultracentrifugation. Annu Rev Biophys Biomol Struct 28:75–100

Laue TM, Anderson AL, Weber BW (1997) Prototype fluorescence detector for the XLA analytical ultracentrifuge. SPIE Proc 2985:196–204

Liu J, Lester P, Builder S, Shire SJ (1995) Characterization of complex formation by humanized anti-IgE monoclonal antibody and monoclonal human IgE. Biochemistry 34(33):10474–10482

Lyons DF, Lary JW, Husain B, Correia JJ, Cole JL (2013) Are fluorescence-detected sedimentation velocity data reliable? Anal Biochem 437(2):133–137

MacGregor IK, Anderson AL, Laue TM (2004) Fluorescence detection for the XLI analytical ultracentrifuge. Biophys Chem 108(1-3):165–185

Olshina MA, Angley LM, Ramdzan YM, Tang J, Bailey MF, Hill AF, Hatters DM (2010) Tracking mutant huntingtin aggregation kinetics in cells reveals three major populations that include an invariant oligomer pool. J Biol Chem 285(28):21807–21816

Pettikiriarachchi A, Gong L, Perugini MA, Devenish RJ, Prescott M (2012) Ultramarine, a chromoprotein acceptor for Förster resonance energy transfer. PLoS One 7(7):e41028

Polling S, Hatters DM, Mok Y (2013) Size analysis of polyglutamine protein aggregates using fluorescence detection in an analytical ultracentrifuge. Methods Mol Biol 1017:59–71

Romanini DW, Cornish VW (2012) Protein labelling: playing tag with proteins. Nat Chem 4(4):248–250

Sanchorawala V (2006) Light-chain (AL) amyloidosis: diagnosis and treatment. Clin J Am Soc Nephrol 1:1331–1341

Schachman HK (1959) Ultracentrifugation in biochemistry. Academic, New York

Schmidt B, Rappold W, Rosenbaum V, Fischer R, Riesner D (1990) A fluorescence detection system for the analytical ultracentrifuge and its application to proteins, nucleic acids, and viruses. Colloid Polym Sci 268(1):45–54

Schuck P (2000) Size distribution analysis of macromolecules by sedimentation velocity ultracentrifugation and Lamm equation modeling. Biophys J 78:1606–1619

Schuck P, Perugini MA, Gonzales NR, Howlett GJ, Schubert D (2002) Size-distribution analysis of proteins by analytical ultracentrifugation: strategies and application to model systems. Biophys J 82(2):1096–1111

Stafford WF, Sherwood PJ (2004) Analysis of heterologous interacting systems by sedimentation velocity: curve fitting algorithms for estimation of sedimentation coefficients, equilibrium and rate constants. Biophys Chem 108(1–3):231–243

Svedberg T, Pedersen KO (1940) The ultracentrifuge. Clarendon, Oxford

Swart C, Haylett W, Kinnear C, Johnson G, Bardien S, Loos B (2014) Neurodegenerative disorders: dysregulation of a carefully maintained balance? Exp Gerontol 58:279–291

Tsien RY (1998) The green fluorescent protein. Annu Rev Biochem 67:509–544

van Holde KE, Hansen JC (1998) Analytical ultracentrifugation from 1924 to present: a remarkable history. Chemtracts Biochem Mol Biol 11:933–941

Vistica J, Dam J, Balbo A, Yikilmaz E, Mariuzza RA, Rouault TA, Schuck P (2004) Sedimentation equilibrium analysis of protein interactions with global implicit mass conservation constraints and systematic noise decomposition. Anal Biochem 326(2):234–256

Wang X, Zhang C, Chiang Y, Toomey S, Power MP, Granoff ME, Richardson R, Xi W, Lee DJ, Chase S, Laue TM, Denis CL (2012) Use of the novel technique of analytical ultracentrifugation with fluorescence detection system identifies a 77S monosomal translation complex. Protein Sci 21(9):1253–1268

Warrick JM, Chan HYE, Gray-Board GL, Chai Y, Paulson HL, Bonini NM (1999) Suppression of polyglutamine-mediated neurodegeneration in Drosophila by the molecular chaperone HSP70. Nat Genet 23(4):425–428

Wilmann PG, Petersen J, Pettikiriarachchi AZ, Rossjohn J, Buckle AM, Smith SC, Olsen S, Perugini MA, Devenish RJ, Prescott M (2005) The 2.1 Å crystal structure of the far-red fluorescent protein HcRed: inherent conformational flexibility of the chromophore. J Mol Biol 349(1):223–237

Wowor AJ, Yu D, Kendall DA, Cole JL (2011) Energetics of SecA dimerization. J Mol Biol 408(1):87–98

Yphantis DA, Lary JW, Stafford WF, Liu S, Olson PH, Hays DB, Moody TP, Ridgeway T, Lyons D, Laue T (1994) On line data acquisition for the Rayleigh interference optical system of the analytical ultracentrifuge. In: Schuster TM, Laue TM (eds) Modern analytical ultracentrifugation: acquisition and interpretation of data for biological and synthetic polymer systems. Birkhauser, Boston, pp 209–226

Zhang C, Wang X, Park S, ChiangY XW, Laue TM, Denis CL (2014) Only a subset of the PAB1-mRNP proteome is present in mRNA translation complexes. Protein Sci 23(8):1036–1049

Zhao C, Hellman LM, Zhan X, Bowman WS, Whiteheart SW, Fried MG (2010) Hexahistidine-tag-specific optical probes for analyses of proteins and their interactions. Anal Biochem 399(2):237–245

Zhao H, Berger AJ, Brown PH, Kumar J, Balbo A, May CA, Casillas E Jr, Laue TM, Patterson GH, Mayer ML, Schuck P (2012) Analysis of high-affinity assembly for AMPA receptor amino-terminal domains. J Gen Physiol 139(5):371–388

Zhao H, Lomash S, Glasser C, Mayer ML, Schuck P (2013) Analysis of high affinity self-association by fluorescence optical sedimentation velocity analytical ultracentrifugation of labeled proteins: opportunities and limitations. PLoS One 8(12):e83439

Zhao H, Ma J, Ingaramo M, Andrade E, MacDonald J, Ramsay G, Piszczek G, Patterson GH, Schuck P (2014a) Accounting for photophysical processes and specific signal intensity changes in fluorescence-detected sedimentation velocity. Anal Chem 86(18):9286–9292

Zhao H, Mayer ML, Schuck P (2014b) Analysis of protein interactions with picomolar binding affinity by fluorescence-detected sedimentation velocity. Anal Chem 86(6):3181–3187